Hindawi Publishing Corporation
Mathematical Problems in Engineering
Volume 2016, Article ID 3070265, 11 pages
http://dx.doi.org/10.1155/2016/3070265

Research Article

Research on Mathematical Model of Composite Micromachining of Laser and Electrolysis Based on the Electrolyte Fluid

Aixi Sun,[1] Bo Hao,[1,2] Yulan Hu,[3] and Dewei Yang[1]

[1]*School of Mechanical Engineering, Nanjing University of Science and Technology, Nanjing 210094, China*
[2]*School of Mechanical Engineering, Shenyang Ligong University, Shenyang 110159, China*
[3]*School of Information Science and Engineering, Shenyang Ligong University, Shenyang 110159, China*

Correspondence should be addressed to Bo Hao; hb1166@126.com

Received 25 September 2015; Revised 16 February 2016; Accepted 17 February 2016

Academic Editor: Francesco Franco

A new technology of composite micromachining of laser and electrolysis is presented through a combination of technological advantages of laser processing and electrolytic machining. The implication of its method is that laser processing efficiently removes metallic materials and that pulse electrolytic machining removes recast layer and controls shape precisely. Machining accuracy and efficiency can be improved. The impacts that electrolyte fluid effectively cools the microstructure edge in the laser machining process and that gas-liquid two-phase flow makes the electrolyte conductivity produce uneven distribution in the electrolytic processing are considered. Some approximate assumptions are proposed on the actual conditions of machining process. The mathematical model of composite micromachining of laser and electrolysis based on the electrolyte fluid is built. The validity of the model can be verified by experimentation. The experimental results show that processing accuracy meets accuracy requirements which are ±0.05 mm. Machining efficiency increases more than 20 percent compared to electrolytic processing.

1. Introduction

Laser processing and electrolytic processing are widely used in manufacturing technology of precision machining of microsystem. Laser micromachining method has the advantages of high efficiency, high precision, and low cost. However, there are still a series of processing defects to be controlled difficultly, such as edge microcrack, heat affected zone, and recast layer [1–7]. Electrolytic micromachining method has the advantages of good surface quality, no heat affected zone, and high machining accuracy. However, there are control problems, such as low machining efficiency, horizontal corrosion, and difficult exclusion of electrolytic products [8–14]. Therefore, it is very necessary to explore a new micromachining method to solve the machining problems of high precision, high efficiency, and high quality of metallic microstructure.

In this paper, a new technology of composite micromachining of laser and electrolysis is presented through a combination of technological advantages of laser processing and electrolytic machining. The implication of its method is that laser processing efficiently removes metallic materials and that pulse electrolytic machining removes recast layer and controls shape precisely. Machining accuracy and efficiency can be improved. It can achieve micron scale machining size and micron scale processing accuracy. It will provide technical support for the micromachining method of microparts in aerospace manufacturing industry with high precision, high efficiency, and low cost.

In order to solve the practical problems, this paper considers the impacts that electrolyte fluid effectively cools the microstructure edge in the laser machining process and that gas-liquid two-phase flow makes the electrolyte conductivity produce uneven distribution in the electrolytic processing. Some approximate assumptions are proposed on the actual conditions of composite micromachining process. The mathematical model of composite micromachining of laser and electrolysis based on the electrolyte fluid is built. The validity of the model is verified by experimentation.

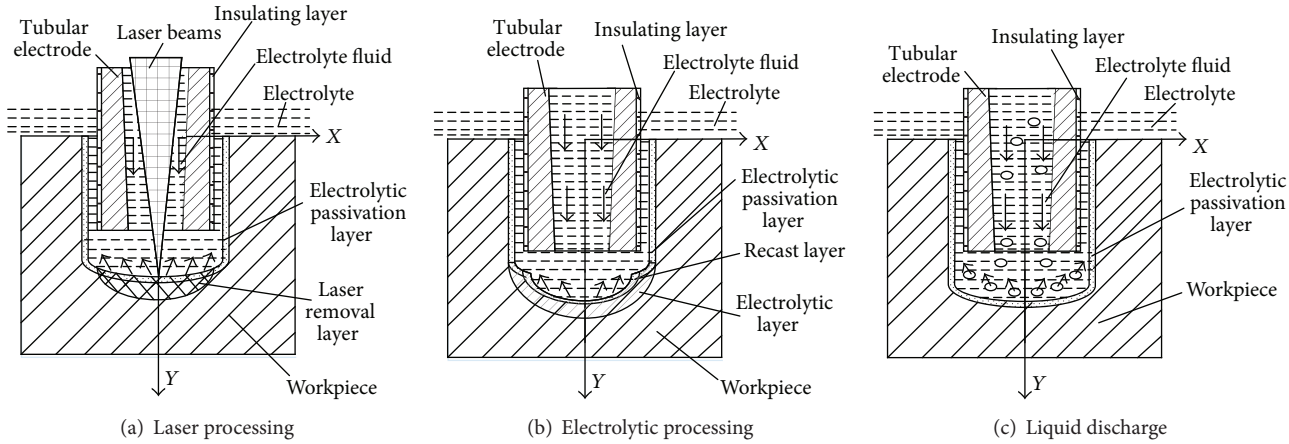

Figure 1: Composite micromachining process model of laser and electrolysis.

2. Composite Micromachining Process Model

In order to reduce the attenuation of laser energy by hydrogen bubble and electrolytic product, composite micromachining method adopts time division control of laser and electrolysis. Negative effects that electrolytic machining has on laser processing can be eliminated.

Composite micromachining process model of laser and electrolysis is shown in Figure 1 and its processing sequence is shown in Figure 2. In the time of T_1, green laser processing based on electrolyte fluid can greatly reduce heat affected zone, thermal deformation, and heat damage to keep original structure of materials. Laser beams can still continue to transfer along the original optical path when the electrolyte fluid is scattered around the surface of the workpiece. Therefore, it can improve locality and accuracy by these methods. In the time of T_2, nonlinear characteristic of η-i curve of current efficiency is strengthened by high frequency microsecond pulse electrolysis power. Electrochemical reaction is limited by side wall insulating tubular electrode on the workpiece area corresponding to the end of electrode. The relative stability of concentration and temperature of electrolyte is maintained by electrolyte system based on PLC. Hydroxide precipitation is not easy to be generated by low concentration of acid composite solution. Pulse electrolytic machining can remove recast layer and control shape precisely by means of these methods. Meanwhile, it makes use of passive film to avoid stray corrosion effectively on the nonprocessing area. So there are these methods that can improve machining stability and precision. In the time of T_3, hydrogen gas bubble and electrolytic processing product can be evacuated from the tubular electrode in order to reduce the attenuation of laser energy. Therefore, composite micromachining can be realized in the time of segmentation with the repeated iteration of laser processing results and electrochemical processing results.

For one thing, there is a part of laser energy that can be used to remove workpiece materials efficiently. The depth of microhole is produced. For another thing, the materials are heated up by another part of laser energy so that their electrochemical dissolution speed can be faster than others. Pulse electrolytic machining removes recast layer and controls shape precisely because of electrochemical anodic dissolution. Machining quality and accuracy can be improved. Time division control can reduce the attenuation of laser energy by hydrogen bubble and electrolytic product. It can eliminate negative effects of laser processing acted on by electrolytic machining. The continuous cooling of materials can greatly reduce thermal effect by electrolyte fluid. It can reduce thermal deformation and heat damage and keep their original structure. Electrolyte fluid can duly discharge electrolytic product, bubble, and Joule heat in machining gap. It can eliminate concentration polarization and equilibrate electrical conductivity. Consequently these means can improve machining efficiency and accuracy.

3. Mathematical Model of Composite Micromachining of Laser and Electrolysis Based on the Electrolyte Fluid

According to the actual conditions of composite micromachining process, some approximate assumptions are proposed. The mathematical model of composite micromachining of laser and electrolysis based on the electrolyte fluid is built. It is based on the temperature field model of laser processing, electric field model of electrolytic machining, flow field model of electrolyte fluid, and their coupling relationship. It can provide theoretical basis for establishing the experimental system of composite micromachining process.

3.1. Mathematical Model of Temperature Field Based on Laser Processing. In order to study temperature field distribution on the surface of workpiece, the following assumptions are put forward [15, 16].

(1) Laser beam in space appears to be on the basic mode of Gaussian distribution.

(2) Workpiece materials are homogeneous mediums with isotropic properties. Physical thermal parameters of materials are constant.

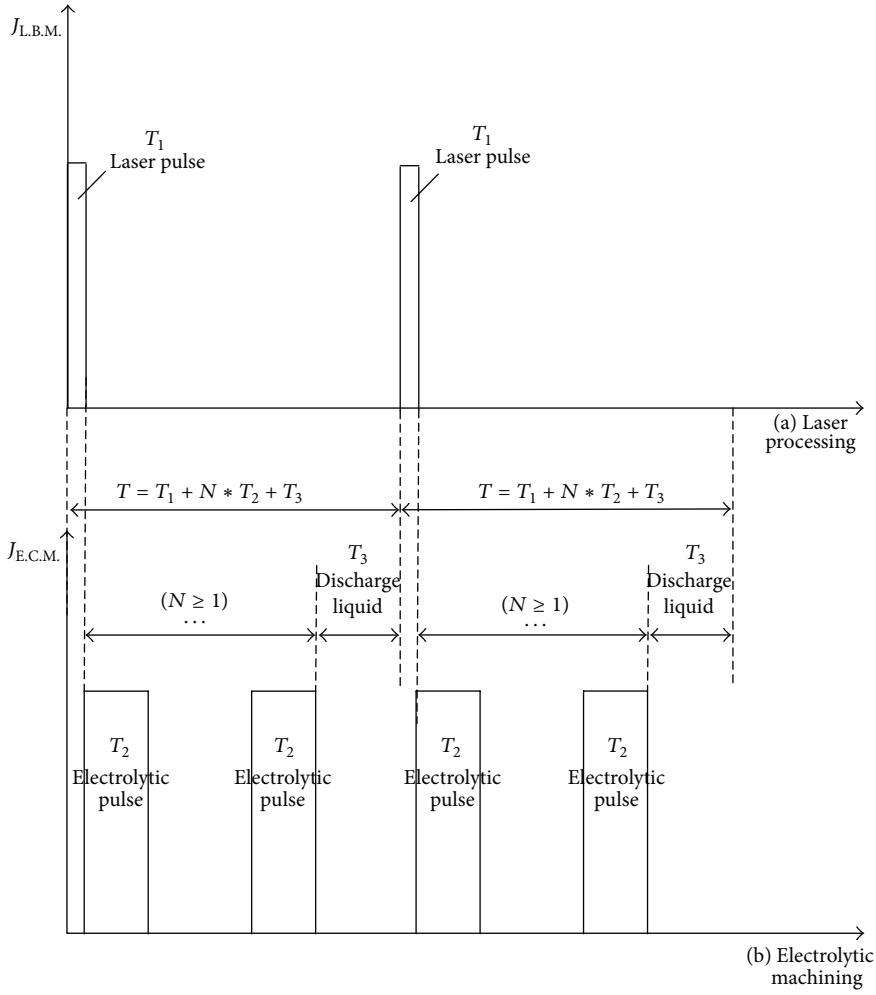

Figure 2: Time sequence of composite micromachining.

(3) Molten metals are removed completely under the action of the rapid expansion of plasma and vapor particles.

(4) Removal of metals by gasification is ignored.

(5) The situation that plasma impacts absorption during laser processing is not considered.

Model of temperature field based on laser processing is shown in Figure 3.

Mathematical model equations of temperature field distribution in the laser micromachining gap is as shown in the following [17, 18]:

$$\rho c \frac{\partial T(x,y,t)}{\partial t} = K \frac{\partial^2 T(x,y,t)}{\partial x^2} + K \frac{\partial^2 T(x,y,t)}{\partial y^2}. \quad (1)$$

The first boundary condition is as follows.

Temperature on the processing boundary is as shown in the following:

$$T(x,y,t=0) = T_0. \quad (2)$$

The second boundary condition is as follows.

Heat flux density of laser source on the processing boundary is as shown in the following [16, 19]:

$$q = A * \frac{2Q}{\pi R^2} \mathrm{EXP}\left(-2\frac{x^2}{R^2}\right) \mathrm{EXP}\left(-u(\lambda) l\right). \quad (3)$$

In the formula, A is laser absorption rate of metallic materials, Q is peak power of laser pulses, R is radius of laser beam waist, x is X axial distance from the center of heat source, $\mu(\lambda)$ is attenuation coefficient of laser in the electrolyte, and l is laser transmission length in the electrolyte.

The third boundary condition is as follows.

The interface condition of phase transition is as shown in the following [16, 17]:

$$-K \frac{\partial T(x,y,t)}{\partial y} = h_c (T - T_0) + \sigma \varepsilon \left(T^4 - {T_0}^4\right). \quad (4)$$

In the formula, h_c is convection heat transfer coefficient of electrolyte fluid, T is materials surface temperature after laser processing, T_0 is initial temperature which is equal to electrolyte temperature, σ is Stefan-Boltzmann constant, and ε is thermal radiation rate of metallic materials.

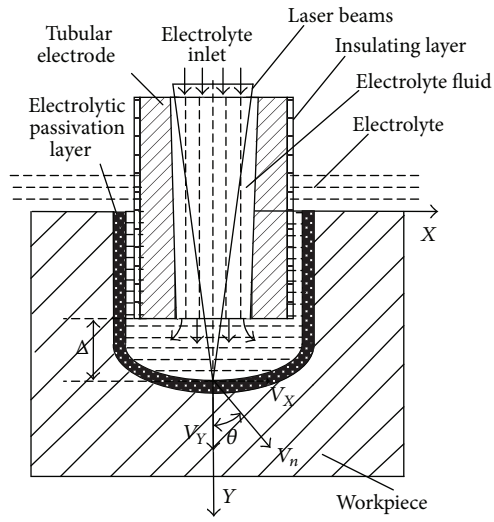

Figure 3: Model of temperature field based on laser processing.

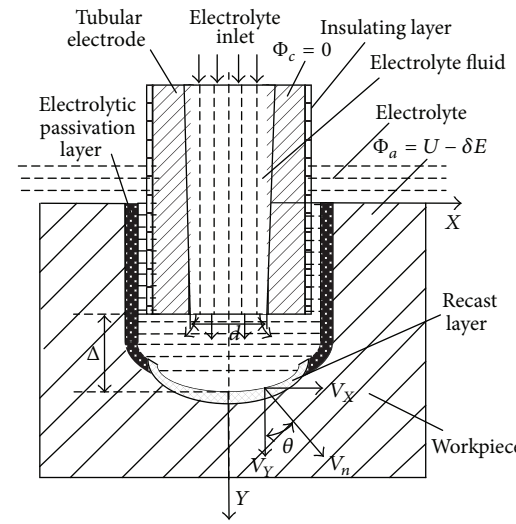

Figure 4: Model of electric field based on electrolytic processing.

Peripheral interface condition of work piece is as shown in the following [16, 17]:

$$-K\frac{\partial T(x,y,t)}{\partial y} = h\left(T - T_0\right) + \sigma\varepsilon\left(T^4 - {T_0}^4\right). \quad (5)$$

In the formula, h is natural convection heat transfer coefficient of electrolyte.

The finite element difference method is used to calculate the above formulas. The temperature field distribution of single laser pulse processing can be acquired. Therefore, section profile of laser micromachining can be obtained by the removal of material above the melting temperature.

3.2. Mathematical Model of Electric Field Based on Electrolytic Processing. In order to study the electric field distribution on the surface of workpiece, the following assumptions are put forward [20–23].

(1) Electric field in machining gap is regarded as electric field in the passive electric conduction medium.

(2) Electrolytic machining has been in a state of balancing process.

(3) Electrolyte is isotropic in the machining process. In other words, the electrical conductivity of electrolyte is the same and constant everywhere.

(4) Anodic electrochemical dissolution obeys Faraday's law. Electric potential distribution is in accord with Laplace equation.

(5) After tubular electrode adsorbs hydrogen and other gases in the machining process, primary battery is formed to produce antielectromotive force. Therefore, voltage drop of electrolyte is regarded as the boundary condition of anode surface to analyse electric field distribution in machining gap.

Model of electric field based on electrolytic processing is shown in Figure 4.

Mathematical model equations of electric potential distribution in electrochemical micromachining gap are as shown in the following:

$$\frac{\partial^2\phi}{\partial x^2} + \frac{\partial^2\phi}{\partial y^2} = 0. \quad (6)$$

Boundary condition of cathode surface is as shown in the following:

$$\phi_c = 0. \quad (7)$$

Boundary condition of anodic surface is as shown in the following:

$$\phi_a = U - \delta E. \quad (8)$$

Electrolytic removal rate of anodic surface is as shown in the following:

$$\begin{aligned} V_x &= \eta\omega\kappa E_x, \\ V_y &= \eta\omega\kappa E_y. \end{aligned} \quad (9)$$

In the formula, U is voltage between cathode and anode, δE is decomposition voltage, V_x and V_y are electrolytic removal velocity components, $\eta\omega$ is actual volume electrochemical equivalent, κ is electrical conductivity of electrolyte, and E_x and E_y are electric field intensity components.

First of all, removal rates of electrolytic processing on the surface of workpiece can be acquired by the above formulas and boundary conditions. Besides, section profile of electrochemical micromachining is obtained by time integration.

3.3. Mathematical Model of Flow Field Based on Electrolyte Fluid. In order to study flow field distribution in composite micromachining gap, the following assumptions are put forward [24].

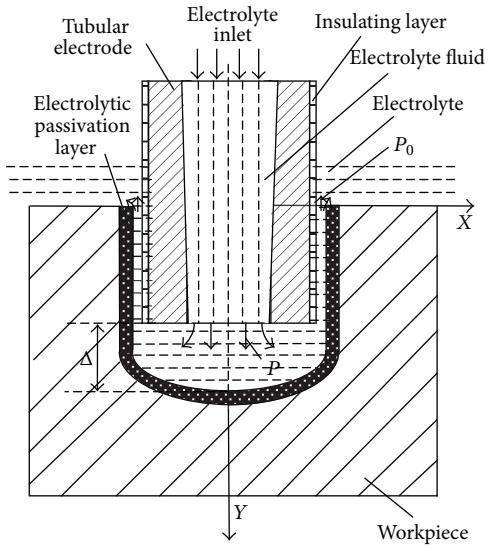

Figure 5: Model of flow field based on electrolyte fluid.

(1) Electrolyte is continuous incompressible viscous fluid.

(2) The energy dissipation caused by the change of medium temperature can be neglected in the machining process. The flow field is constrained by mass conservation equation and momentum conservation equation.

(3) In the case of high strain rate and larger streamline bending degree, the effects of rotation in mean flow and swirl flow acted on by turbulent flow and low Reynolds number are considered to better deal with the flow.

(4) The influence of gravity is ignored because the machining gap is very small.

Model of flow field based on electrolyte fluid is shown in Figure 5.

Mass conservation equation of incompressible viscous fluid is as shown in the following [25, 26]:

$$\frac{\partial(\rho u)}{\partial x} + \frac{\partial(\rho v)}{\partial y} = 0. \tag{10}$$

In the formula, ρ is electrolyte density and u and v are speed components.

Momentum conservation equation of incompressible viscous fluid is as shown in the following [23]:

$$\begin{aligned} \frac{\partial(\rho u)}{\partial t} + \nabla(\rho u\overline{u}) &= -\frac{\partial p}{\partial x} + \frac{\partial \tau_{xx}}{\partial x} + \frac{\partial \tau_{yx}}{\partial y} + F_x, \\ \frac{\partial(\rho v)}{\partial t} + \nabla(\rho v\overline{u}) &= -\frac{\partial p}{\partial y} + \frac{\partial \tau_{xy}}{\partial x} + \frac{\partial \tau_{yy}}{\partial y} + F_y. \end{aligned} \tag{11}$$

In the formula, p is pressure, τ_{xx}, τ_{xy}, and τ_{yy} are viscous stress components, and F_x and F_y are mass force components.

The transport equation of RNG k-ε turbulence model of electrolyte in machining gap is as shown in the following [24]:

$$\begin{aligned} \frac{\partial(\rho k)}{\partial t} + \frac{\partial(\rho k u_i)}{\partial x_i} &= \frac{\partial}{\partial x_j}\left[\left(\mu + \frac{\mu_t}{\delta_k}\right)\frac{\partial k}{\partial x_j}\right] + G_k \\ &\quad - \rho\varepsilon, \\ \frac{\partial(\rho\varepsilon)}{\partial t} + \frac{\partial(\rho\varepsilon u_i)}{\partial x_i} &= \frac{\partial}{\partial x_j}\left[\left(\mu + \frac{\mu_t}{\delta_\varepsilon}\right)\frac{\partial \varepsilon}{\partial x_j}\right] + \frac{C_{1\varepsilon}}{k}G_k \\ &\quad - C_{2\varepsilon}\rho\frac{\varepsilon^2}{k} - R_\varepsilon. \end{aligned} \tag{12}$$

In the formula, $R_\varepsilon = (C_\mu\rho\eta^3(1-\eta/\eta_0)/(1+\beta\eta^3))(\varepsilon^2/k)$, $\eta = (2S_{ij}S_{sj})^{1/2}(k/\varepsilon)$, $S_{sj} = (1/2)(\partial u_s/\partial x_j + \partial u_j/\partial x_s)$, $\eta_0 = 4.38$, $\beta = 0.012$, $C_\mu = 0.0845$, $C_{1\varepsilon} = 1.42$, $C_{2\varepsilon} = 1.68$, $\sigma_k = 1.0$, $\sigma\varepsilon = 1.3$, k is turbulent kinetic energy, ε is dissipation rate of turbulent kinetic energy, u_i is time-averaged velocity, μ_t is turbulent viscosity, and G_k is the generation of turbulent kinetic energy caused by average velocity gradient.

The distribution of electrolyte pressure on the surface of workpiece is obtained by the above formulas and boundary conditions.

3.4. The Coupled Model of Temperature Field and Flow Field of Laser Processing Based on Electrolyte Fluid. The comparison of heat conduction of workpiece in the laser machining process is shown in Figure 6. The traditional laser processing must produce heat affected zone and thermal deformation. Laser processing based on electrolyte fluid makes use of electrolyte fluid to effectively cool the edge of microstructure in the machining process. The heat is duly taken away from the ablation zone of microstructure in the first laser pulse interval so that the heat cannot be further conducted to the workpiece. Therefore, thermal deformation and heat damage of materials can be greatly reduced to keep their original structure [27].

In the laser machining process, the changes of convection heat transfer coefficient are caused by pressure changes of electrolyte fluid. It has an influence on laser processing forming. Consequently, the coupling relationship between temperature field and flow field takes convection heat transfer coefficient as a coupling variable, which is shown in the following [16, 28]:

$$h_c = \frac{K_{\text{wat}}}{L}\text{Nu}. \tag{13}$$

In the formula, $\text{Nu} = 0.7212\text{Pr}^{0.37}\text{Re}^{0.5}$, $\text{Pr} = \mu C_P/K_{\text{wat}}$, $\text{Re} = v_{\text{wat}}D_h/\nu$, $v_{\text{wat}} = \sqrt{(2*P)/\rho_w}$, K_{wat} is thermal conductivity of electrolyte, L is characteristic size of electrolyte fluid, Nu is Nusselt number of electrolyte, Pr is Prandtl number, Re is Reynolds number, μ is dynamic viscosity of electrolyte, C_P is isobaric specific heat of electrolyte, v_{wat} is average velocity of electrolyte fluid, D_h is hydraulic diameter of electrolyte fluid, ν is kinematic viscosity coefficient of electrolyte fluid, P is electrolyte pressure, and ρ_w is electrolyte density.

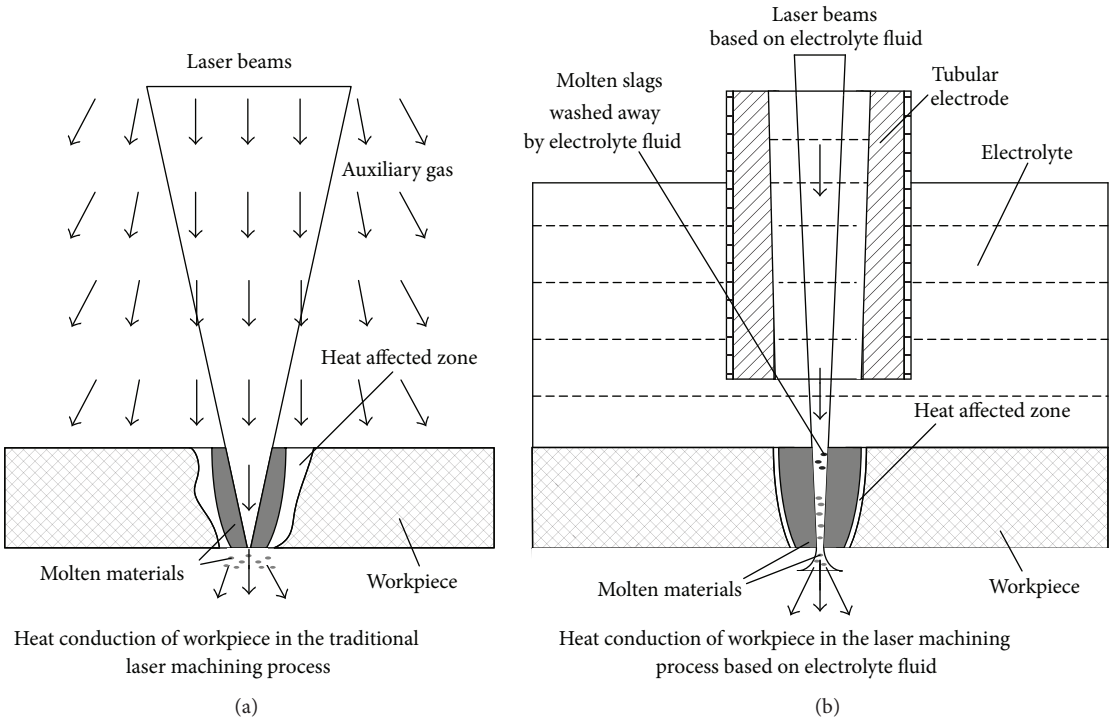

Figure 6: The comparison of heat conduction of workpiece in the laser machining process.

3.5. The Coupled Model of Electric Field and Flow Field of Electrolytic Machining Based on Gas-Liquid Two-Phase Flow. In the electrolytic machining process, hydrogen gas is produced on the cathode. Electrolytic products, oxygen gas, and other gases are produced because of anodic dissolution. It is not considered that small volume ratio of electrolytic products has an influence on electrical conductivity and density of electrolyte. Therefore, the case can be simplified as gas-liquid two-phase flow. Model of gas-liquid two-phase flow in machining gap is shown in Figure 7. The following assumptions are put forward [20, 23].

(1) Electrolytic processing has been in a state of equilibrium. Machining gap has reached balance gap. Anodic corrosion rate is equal to cathode feed speed. Heat exchange of electrolyte and tool electrodes has been in balance state.

(2) The surfaces of cathode and anode are equal potential surfaces. Nonlinear mutation of electrode potential approximates to decomposition voltage at the interface of electrodes and solution. The electrical potential gradient is the same in the direction perpendicular to flow speed of electrolyte.

(3) The liquid phase cannot be compressed in the machining gap. The changes of gas phase state obey the ideal gas state equation. There is no mass transfer between two phases. Air bubble is uniform distribution in liquid phase. Phase parameters of cross sections are equal along the flow direction.

The generated gases are uniformly mixed in the electrolyte flowing through the machining gap, which is in the form of small air bubbles. Gas-liquid two-phase flow can be produced. Electrical conductivity of electrolyte decreases with the increase of gas content. At the same time, it produces uneven distribution because of Joule heat generated by machining current. After a certain transient process, electrolyte temperature is in a stable state. That is to say, it is steady state temperature field. In order to simplify the

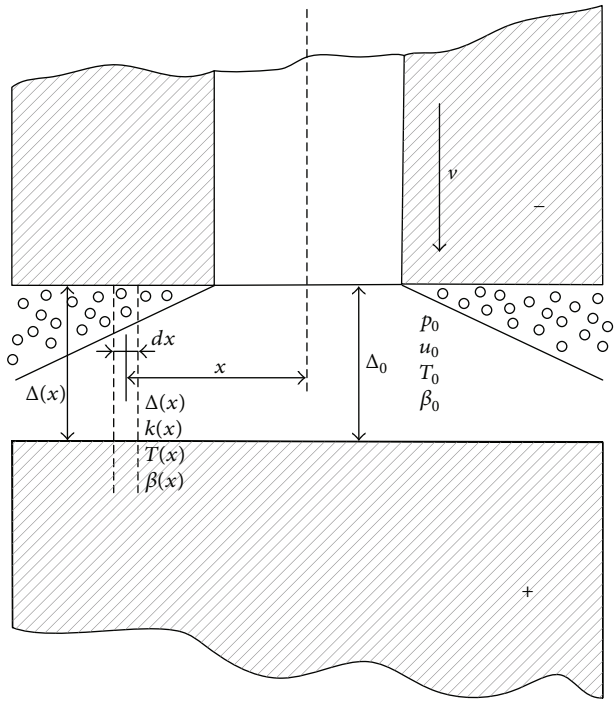

Figure 7: Model of gas-liquid two-phase flow in machining gap.

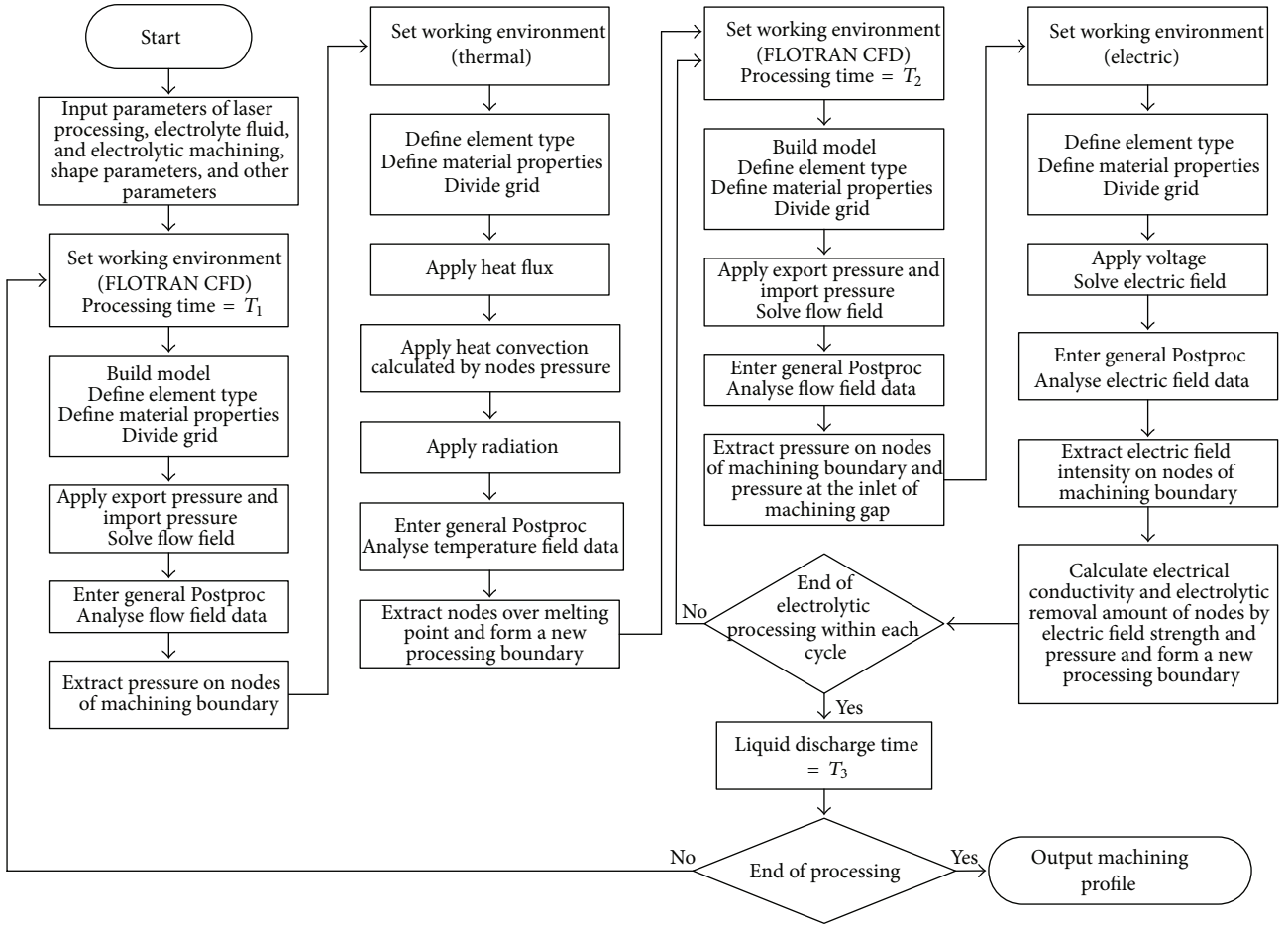

Figure 8: Numerical simulation process of experimental system of composite micromachining process.

problem, the effect of temperature on electrical conductivity is neglected. The coupling relationship of electric field and flow field of electrolytic machining based on gas-liquid two-phase flow is as shown in the following [20, 23]:

$$\kappa = \kappa_0 \left(1 - \beta\right)^{1.5}. \tag{14}$$

In the formula, $\beta = b_g R_g T|x|/(b_g R_g T|x| + \Delta_0 u_0 p)$, $T = T_0 + a_T|x|$, $a_T = \kappa_0 E^2/\rho_1 C_1 u_0$, $b_g = \eta_g k_g i$, $i = \kappa_0 E$, $\Delta_0 = (U - \delta E)/E$, κ_0 is electrical conductivity at the inlet, β is bubble ratio, R_g is gas state constant of hydrogen gas, T_0 is initial temperature of electrolyte, ρ_1 is electrolyte density, C_1 is specific heat of electrolyte, η_g is current efficiency of hydrogen evolution which is equal to electrolytic machining efficiency expressed by "η," k_g is electrochemical equivalent of hydrogen evolution, i is current density, Δ_0 is machining gap of cross section of process x, E is electric field intensity, u_0 is flow speed at the inlet of machining gap, and p is pressure.

4. Experiments of Composite Micromachining Process

According to mathematical model of composite micromachining process, APDL is used to establish the experimental system, which is the abbreviation for "ANSYS parametric design language." Its forming law is analyzed on the basis of temperature cloud chart of laser processing and electric field intensity cloud chart of electrolytic machining. The validity of its mathematical model is verified from the aspects of machining precision and efficiency.

4.1. Numerical Simulation Process of Experimental System of Composite Micromachining Process. Numerical simulation process of experimental system of composite micromachining process is shown in Figure 8. APDL was used to establish its experimental system. Thermal module, FLOTRAN CFD module, and electric module could be called on the platform of ANSYS system to conduct the simulation of its experimental system. The initial boundary of electrolytic machining was achieved by simulation results of laser processing. Final machining profile could be obtained by repeated iteration between the results of laser processing and the results of electrolytic machining.

4.2. Experimental Verification of Composite Micromachining Process. In the process of laser machining, convection heat transfer coefficient was calculated according to pressure of electrolyte fluid. The temperature field distribution on the

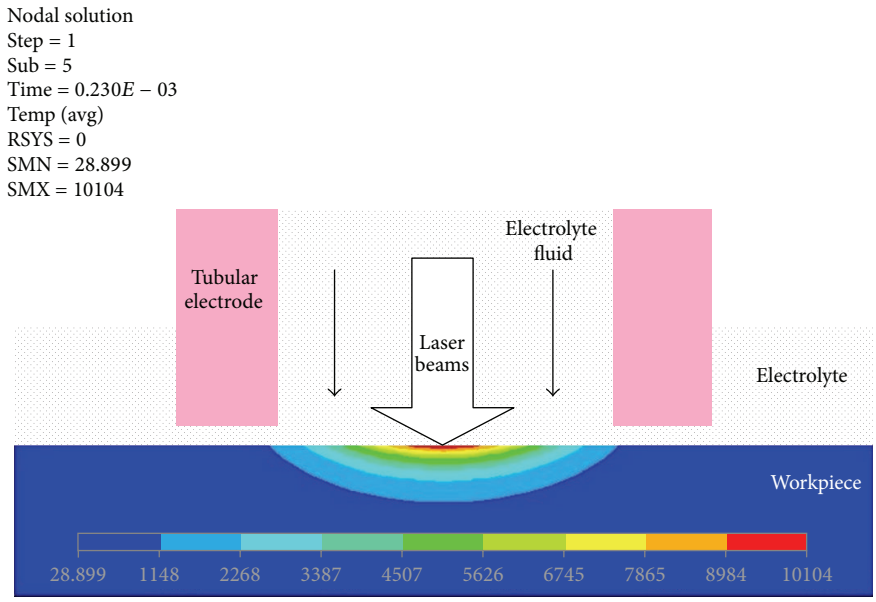

Figure 9: Temperature cloud chart on the surface of workpiece in the first laser pulse processing.

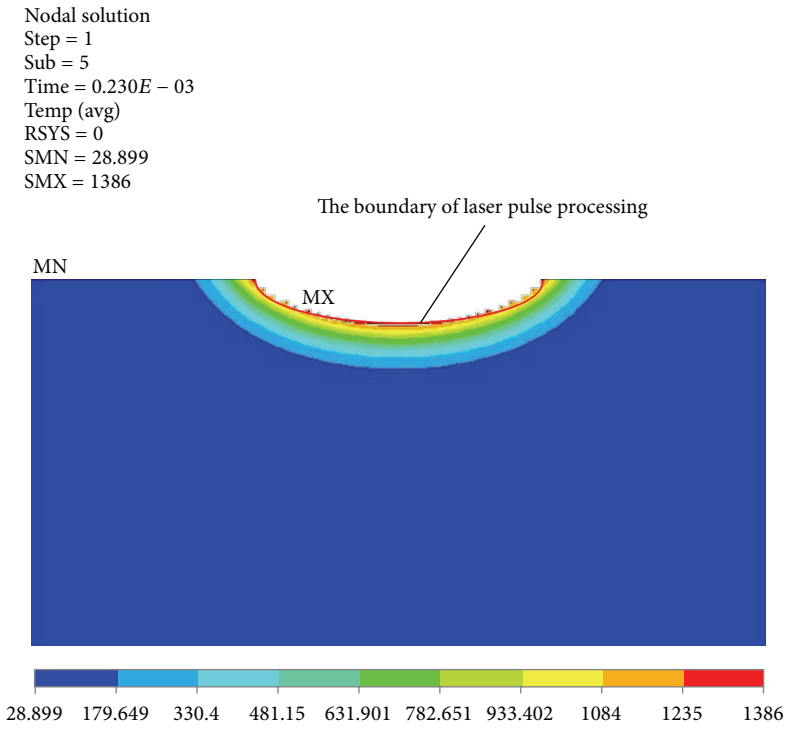

Figure 10: The boundary after the first laser pulse processing.

surface of workpiece was obtained by applying heat flux and other loads. Temperature cloud chart on the surface of workpiece was shown in Figure 9, which was acted on by 300 mJ laser energy in the first laser pulse processing. Its center temperature reached more than ten thousand degrees centigrade, which exceeded melting point and boiling point of 0Cr18Ni9 stainless steel. Therefore, the elements over melting point were removed as molten material of laser processing. The boundary of remaining material was the initial boundary of pulse electrochemical machining in the time of T_2. The boundary after the first laser pulse processing is shown in Figure 10.

Electric field intensity cloud chart on the surface of workpiece was shown in Figure 11, which was acted on by 12.08 V electrolysis voltage in the first laser pulse interval. The electric field intensity of the workpiece region corresponding to

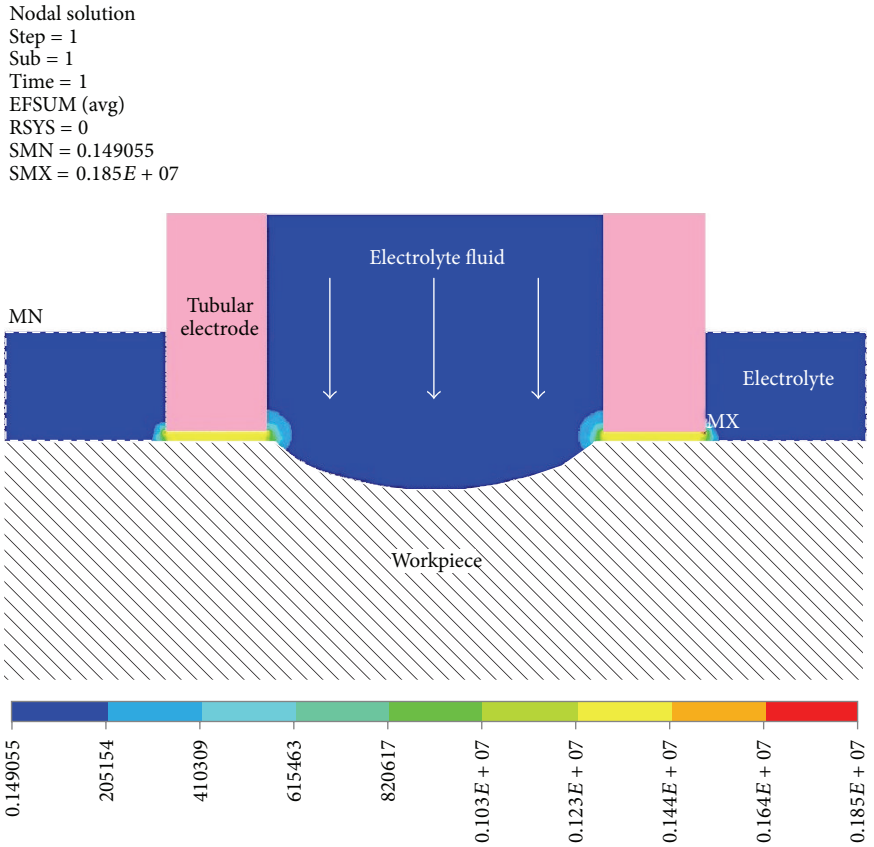

Figure 11: Electric field intensity cloud chart on the surface of workpiece in the first laser pulse interval.

Table 1: The process parameters of composite micromachining and its experimental results.

Process parameters	Laser pulse energy (J)	Laser pulse frequency (Hz)	Electrode feed rate (um/s)	Initial machining gap (um)	Electrolysis voltage (V)	Duty cycle of pulse power (%)	Frequency of pulse power (KHz)	Electrolyte fluid pressure (MPa)	Machining accuracy (um)	Material removal rate (ug/s)
Value	0.3	1	42	8	12.08	0.64	12	0.46	49	87.99

electrode end was larger than others, where the dissolution rate of the materials was faster than others. Among them, the electric field intensity of the workpiece region corresponding to the center of electrode end was maximum. Its value was up to 1322500 V/m. The dissolution rate was the fastest speed. Electric field intensity cloud chart of electrochemical machining in the first laser pulse interval and radial electric field strength distribution diagram on the surface of workpiece were shown in Figure 12. The farther the distance from both sides of the electrode was, the smaller the electric field intensity was. So the dissolution rate of the material also slowed down. Electrical conductivity and current density were calculated by electric field strength and pressure on the boundary of workpiece. The actual displacement of nodes was obtained and the initial boundary of the next pulse electrolytic machining was formed.

The process parameters of composite micromachining and its experimental results were shown in Table 1. Insulating layer limited electric field distribution of side wall of tubular electrode to reduce stray corrosion and to improve machining locality. Its processing accuracy reached 49 um. It met accuracy requirements which are ±0.05 mm. Electrochemical reaction could be limited in the workpiece area corresponding to the end of electrode. The materials from its region were removed. Workpiece boundary of composite machining after 1 second was shown in Figure 13. Anodic dissolution region of pulse electrolytic machining mainly concentrated in the hole wall, where recast layer was efficiently removed. The electrode

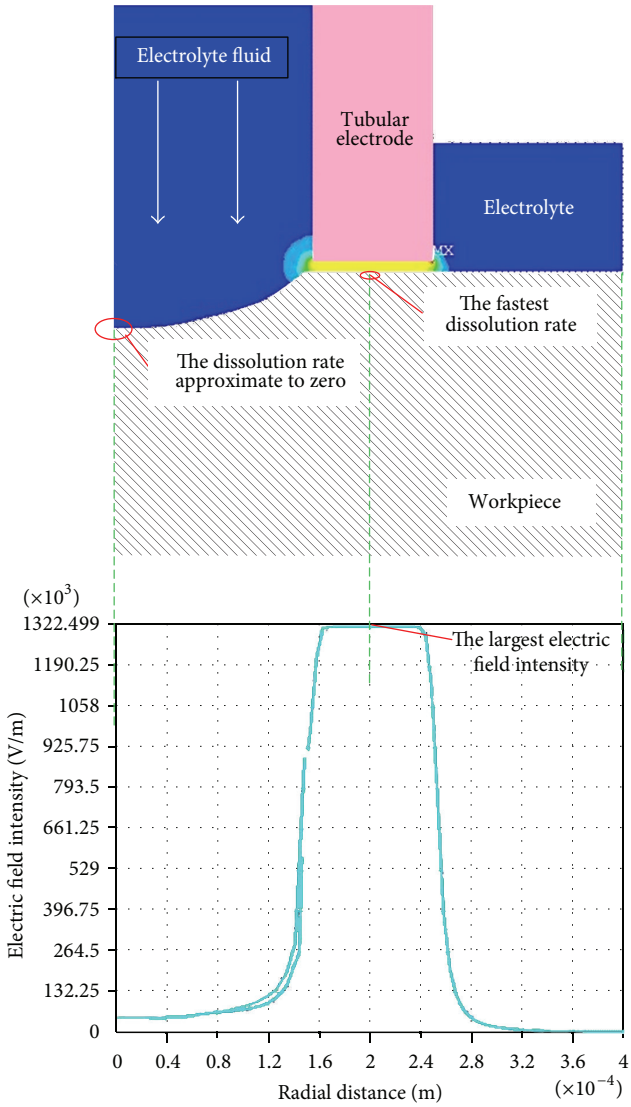

Figure 12: Electric field intensity cloud chart of electrochemical machining in the first laser pulse interval and radial electric field strength distribution diagram on the surface of workpiece.

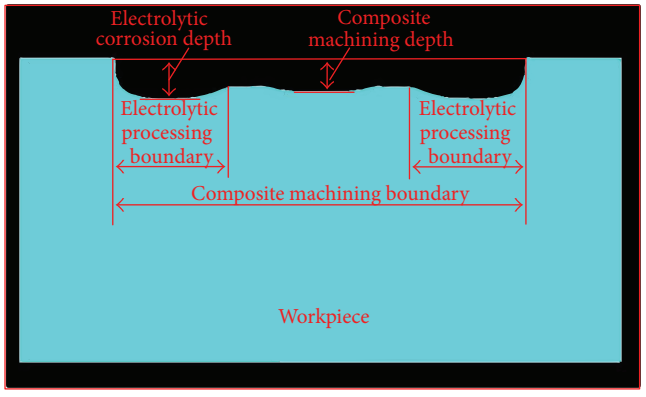

Figure 13: Workpiece boundary of composite machining after 1 second.

feed rate of electrochemical machining was 15 um/s. The geometric scale of side wall insulating tubular electrode was that internal diameter was 0.15 mm and external diameter was 0.5 mm. Other process parameters were the same as composite micromachining. Its material removal rate was 66.22 ug/s. The material removal rate of composite micromachining was 32.87% higher than electrochemical machining. Process requirements could be met where machining efficiency increased more than 20 percent compared to electrolytic processing. Therefore, it is the forming law of composite micromachining that microsecond pulse laser processing efficiently removes metallic materials on the machining area and that microsecond pulse electrolytic machining efficiently removes recast layer in the hole wall and controls shape precisely.

5. Conclusion

The following is a summary of the conclusions.

(1) In this paper, a new technology of composite micromachining of laser and electrolysis is presented through a combination of technological advantages of laser processing and electrolytic machining. The implication of its method is that laser processing efficiently removes metallic materials and that pulse electrolytic machining removes recast layer and controls shape precisely. It can solve the micromachining problems of high precision, high efficiency, and low cost of metallic microstructure in manufacturing technology of microsystem. It will lay the technical foundation for the development of new composite micromachining method of laser and electrolysis.

(2) The effects where electrolyte fluid effectively cools the microstructure edge and gas-liquid two-phase flow makes the electrolyte conductivity produce uneven distribution are considered in the composite micromachining. Some approximate assumptions of its actual conditions are proposed. Based on the temperature field model, electric field model, flow field model, and their coupling relationship, the mathematical model of composite micromachining of laser and electrolysis based on the electrolyte fluid is built. It can provide theoretical basis for establishing the experimental system of composite micromachining process.

(3) According to the mathematical model, the experimental system of composite micromachining process is established. By the experimental verification, the processing accuracy meets accuracy requirements which are ±0.05 mm. The machining efficiency increases more than 20 percent compared to electrolytic processing. Therefore, the validity of its mathematical model is demonstrated.

(4) It is the forming law of composite micromachining that microsecond pulse laser processing based on the electrolyte fluid efficiently removes metallic materials on the machining area and that microsecond pulse electrolytic machining efficiently removes recast layer in the hole wall and controls shape precisely.

To sum up, this paper presents a new technology of composite micromachining of laser and electrolysis. The mathematical model of composite micromachining of laser and electrolysis based on the electrolyte fluid is built, of which the validity is demonstrated by experiment. It will lay the

technical foundation for the development of new composite micromachining method of laser and electrolysis.

Competing Interests

The authors declare that they have no competing interests regarding the publication of this paper.

References

[1] B. Richerzhagen, "Chip singulation process with a water jet-guided laser," *Solid State Technology*, vol. 44, no. 4, pp. 44–49, 2001.

[2] C.-F. Li, D. B. Johnson, and R. Kovacevic, "Modeling of water-jet guided laser grooving of silicon," *International Journal of Machine Tools & Manufacture*, vol. 43, no. 9, pp. 925–936, 2003.

[3] N. Dushkina, F. Wagner, C. Boillat, J.-M. Buchilly, and B. Richerzhagen, "Water jet guided laser versus saw dicing," in *Photon Processing in Microelectronics and Photonics II*, vol. 4977 of *Proceedings of SPIE*, pp. 75–85, 2003.

[4] F. R. Wagner, C. Boillata, J. M. Buchilly et al., "High-speed cutting of thin materials with a Q-switched laser in a water-jet vs. conventional laser cutting with a free running laser," in *Photon Processing in Microelectronics and Photonics II*, vol. 4977 of *Proceedings of SPIE*, pp. 70–71, 2003.

[5] Y. Wang, L. Li, L. Yang, and J. Chu, "Experimental research on water-jet guided laser processing," in *Fundamental Problems of Optoelectronics and Microelectronics III, 659525*, vol. 6595 of *Proceedings of SPIE*, 6 pages, The International Society for Opitcal Engineering, March 2007.

[6] Y. Jihong, *Action Mechanism and Technics Study of Using Laser Drilling Microhole*, Tianjin University, 2008.

[7] B. Xu, X.-Y. Wu, F. Luo, C.-L. Du, and X.-Q. Sun, "Ablation of 0Cr18Ni9 stainless steel films by femtosecond laser," *Optics and Precision Engineering*, vol. 20, no. 1, pp. 45–51, 2012.

[8] G. Chryssolouris and M. Wollowitz, "Electrochemical hole making," *CIRP Annals—Manufacturing Technology*, vol. 33, no. 1, pp. 99–104, 1984.

[9] V. K. Jain, P. G. Yogindra, and S. Murugan, "Prediction of anode profile in ECBD and ECDoperations," *International Journal of Machine Tools and Manufacture*, vol. 27, no. 1, pp. 113–134, 1987.

[10] J. Kozak, K. P. Rajurkar, and R. Balkrishna, "Study of electrochemical jet machining process," *Journal of Manufacturing Science and Engineering*, vol. 118, no. 4, pp. 490–498, 1996.

[11] S. Sharma, V. K. Jain, and R. Shekhar, "Electrochemical drilling of inconel superalloy with acidified sodium chloride electrolyte," *International Journal of Advanced Manufacturing Technology*, vol. 19, no. 7, pp. 492–500, 2002.

[12] M. Datta and D. Landolt, "Fundamental aspects and applications of electrochemical microfabrication," *Electrochimica Acta*, vol. 45, no. 15-16, pp. 2535–2558, 2000.

[13] Y. Liu, D. Zhu, Y.-B. Zeng, S.-F. Huang, and H.-B. Yu, "Experimental investigation on electrochemical micromachining of complex shape parts," *Key Engineering Materials*, vol. 419-420, pp. 425–428, 2010.

[14] H. Chen, Z.-L. Wang, Z.-L. Peng, and W.-S. Zhao, "Fabrication of micro structures by ultra short voltage pulse electrochemical machining," *Key Engineering Materials*, vol. 419-420, pp. 813–816, 2010.

[15] S. Tosto, "Modeiing and computer simuiation of pulsed-laser-induced abiation," *Applied Physics A: Materiais Science & Processing*, vol. 68, no. 4, pp. 439–446, 2002.

[16] Y. Lixin, *Research on System and Techniques of Hybrid Processing of Laser Beam Machining with Jet Electrochemical Machining*, Nanjing University of Aeronautics and Astronautics, 2013.

[17] S. Linsen, S. Guoquan, and L. Zhanguo, "Simulation on laser drilling temperature field by using ANSYS," *Journal of Changchun University of Science and Technology*, vol. 29, no. 4, pp. 19–21, 2006.

[18] F. Yunsong and L. Xiaoxia, "Numerical simulation of temperature field of quartz glass irradiated by pulsed laser based on ANSYS," *Physics Experimentaion*, vol. 32, no. 2, pp. 35–37, 2012.

[19] Y. Wei, L. Zhanguo, and C. Yunguang, "Simulation of temperature field of laser cutting based on ANSYS," *Journal of Changchun University*, vol. 23, no. 12, pp. 1561–1564, 2013.

[20] X. Jiawen, Y. Naizhang, W. Jianye et al., *Electrochemical Machining Technology—Theory, Process and Application*, National Defense Industry Press, Beijing, China, 2008.

[21] Li. Zhiyong and Di. Zhu, "Sun Chunhua, et al. Study on Finite-Element Arithmetic," in *in E1ectrochemical Machining for Turbine Blades[J]*, vol. 15, pp. 1151–1154, China Mechanical Engineering, 2004.

[22] W. Lei and Z. Di, "Determination of anode shape based on finite element method in electrochemical machining," *China Mechanical Engineering*, vol. 17, no. 9, pp. 927–930, 2006.

[23] W. Lisheng, *Multiphysics Problem Simulation Technology and Its Application in Electrochemical Machining Process for Connecting Rod Mold*, HeFei University of Technology, 2011.

[24] F. Xiuqing, K. Min, Y. Yong et al., "Research on flow field simulation and experiment of NC-ECM with spherical cathode," *China Mechanical Engineering*, vol. 24, no. 8, pp. 1038–1042, 2013.

[25] J.-M. Wu and J.-W. Xu, "Numerical simulation of flow field of NC-electrochemical contour evolution machining based on CFD technology," *Journal of System Simulation*, vol. 21, no. 1, pp. 73–75, 2009.

[26] W. Jianmin and X. Jiawen, "Numerical simulation of three—dimensional flow field of cathode of NC-electrochemical machining in machining integral impeller," *China Mechanical Engineering*, vol. 20, no. 7, pp. 780–783, 2009.

[27] L. Ling, *Study on water-jet guided laser micromachining technology [Ph.D. thesis]*, Harbin Institute of Technology, 2008.

[28] L. Chunqi, *Research on Water-Jet Guided Laser Micromachining System and Key Technologies*, Harbin Institute of Technology, Harbin, China, 2012.